Dalton Transactions

PAPER

View Article Online
View Journal | View Issue

Cite this: *Dalton Trans.*, 2016, **45**, 4659

Positional isomerism makes a difference: phosphonic acid anchoring ligands with thienyl spacers in copper(I)-based dye-sensitized solar cells†

Y. Maximilian Klein, Markus Willgert, Alessandro Prescimone, Edwin C. Constable* and Catherine E. Housecroft*

With the aim of improving the photoconversion efficiencies of heteroleptic $[Cu(L_{anchor})(L_{ancillary})]^+$ dyes in n-type dye-sensitized solar cells (DSCs), the previously favoured anchor ((6,6′-dimethyl-[2,2′-bipyridine]-4,4′-diyl)bis(4,1-phenylene))bis(phosphonic acid) (**1**) has been replaced by analogues **2** and **3** containing 2-thienyl spacers between the 2,2′-bipyridine metal-binding domain and the phosphonic acid anchoring groups. The synthesis and characterization of **2** and **3** (2-thienyl spacer with phosphonic acid in the 5- and 4-positions, respectively) are reported. A stepwise, on-surface method was used to assemble $[Cu(L_{anchor})(L_{ancillary})]^+$ dyes onto FTO/TiO_2 electrodes with L_{anchor} = **1**, **2** or **3**, and $L_{ancillary}$ = 6,6′-bis(trifluoromethyl)-2,2′-bipyridine (**4**), 6-trifluoromethyl-2,2′-bipyridine (**5**), 6,6′-dimethyl-2,2′-bipyridine (**6**), and 6-methyl-2,2′-bipyridine (**7**). Changing the solvent in the dye-bath from CH_2Cl_2 to acetone had only a small effect on the photoconversion efficiencies of $[Cu(\mathbf{1})(\mathbf{4})]^+$, $[Cu(\mathbf{1})(\mathbf{5})]^+$ and $[Cu(\mathbf{1})(\mathbf{6})]^+$; the optimal dye in this series was $[Cu(\mathbf{1})(\mathbf{5})]^+$. Comparable DSC performances were achieved by using either anchor **1** or **2**, but there is improved electron injection if the phosphonic acid group is in the 4- rather than 5-position of the thienyl ring (*i.e.* anchor **3** is superior to **2**). Similar open-circuit voltages (V_{OC}) are achieved on going from **1** to **3** with a given $L_{ancillary}$; although there is typically a gain in short-circuit current denisty (J_{SC}) on going from **1** or **3** to **2**, there is an ≈50–60 mV drop in V_{OC} on introducing **2** as the anchor. The best photoconversion efficiencies are obtained for the dye $[Cu(\mathbf{3})(\mathbf{5})]^+$ (η = 2.40% relative to an N719 reference of 5.76%). The conclusions reached from plots of current-density (J) against potential (V), and external quantum efficiency spectra are supported by electrochemical impedance spectroscopic measurements.

Received 13th January 2016,
Accepted 2nd February 2016

DOI: 10.1039/c6dt00166a

www.rsc.org/dalton

Introduction

Recent improvements in the performance of copper-based dye-sensitized solar cells (DSCs) have highlighted the realistic prospect of future DSCs utilizing Earth-abundant metals such as copper[1] and iron[2] rather than rare and expensive metals such as ruthenium. Breaking the 3%[3] then 4%[4] barriers of photoconversion efficiencies of DSCs containing copper(I) sensitizers has provided significant impetus to this research field. In order to tune the properties of copper(I) sensitizers and build into their design electronic 'push–pull' features, heteroleptic complexes of the type shown in Scheme 1 are desirable. However, isolating heteroleptic $[Cu(L_{anchor})(L_{ancillary})]^+$ dyes is hampered by their tendency in solution to form equilibrium mixtures with the homoleptic $[Cu(L_{anchor})_2]^+$ and $[Cu(L_{ancillary})_2]^+$ complexes. To overcome this problem, Odobel and coworkers have focused attention on the advantages of the HETPHEN approach (HETPHEN = heteroleptic bisphenanthroline),[4–6] and we have developed a 'surfaces-as-ligands, surfaces-as-complexes' strategy in which the heteroleptic complex (Scheme 1 and eqn (1)) is assembled directly on the semiconductor surface.[1,7] The latter provides a flexible means of combining a wide range of ancillary ligands with a given anchoring domain, allowing the benefits of different ligand combinations in a $[Cu(L_{anchor})(L_{ancillary})]^+$ dye (Scheme 1) to be rapidly recognized.

Department of Chemistry, University of Basel, Spitalstrasse 51, CH-4056 Basel, Switzerland. E-mail: catherine.housecroft@unibas.ch

†Electronic supplementary information (ESI) available: Synthesis of precursors. Fig. S1–S4: additional NMR spectra; Scheme S3: competing reactions in the conversion of 4,4′-bis(5-bromothiophen-2-yl)-6,6′-dimethyl-2,2′-bipyridine to **2a**, and characterization data of side-products; Fig. S5 ORTEP figure of 4,4′-bis(thiophen-2-yl)-6,6′-dimethyl-2,2′-bipyridine; Fig. S6–S8: additional *J*–*V* curves and EQE spectra; Table S1: parameters for DSCs with N719; Tables S2 and S3: DSC parameters; Tables S4 and S5: EIS data. CCDC 1435291 and 1436307. For ESI and crystallographic data in CIF or other electronic format see DOI: 10.1039/c6dt00166a

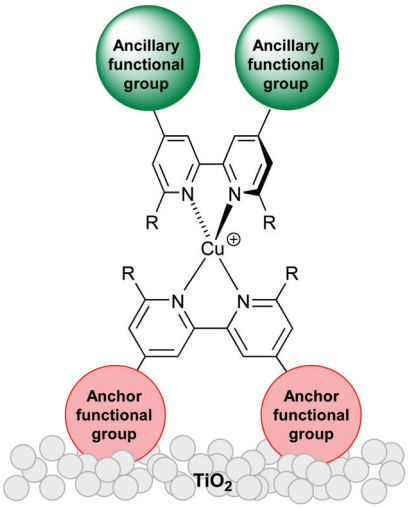

Scheme 1 Schematic illustration of a TiO_2-electrode surface functionalized with a heteroleptic $[Cu(L_{anchor})(L_{ancillary})]^+$ dye.

$$\begin{array}{l} TiO_2\text{-electrode} + L_{anchor} \longrightarrow TiO_2/L_{anchor} \\ \qquad\qquad\qquad\qquad\qquad\quad \rightleftharpoons [Cu(L_{ancillary})_2]^+ \\ \qquad\qquad\qquad\qquad\qquad\quad -\ L_{ancillary} \\ TiO_2/[(L_{anchor})Cu(L_{ancillary})]^+ \end{array} \quad (1)$$

The use of phosphonic acid anchors for copper(I) sensitizers leads to enhanced DSC performance with respect to analogues with carboxylic acid anchors.[8] Grätzel has also described the advantages of phosphonic acid anchors in ruthenium sensitizers,[9] and Meyer and coworkers have shown that in $[Ru(bpy)_3]^{2+}$-based sensitizers, use of 4,4′-$\{(HO)_2OP\}_2$-bpy (bpy = 2,2′-bipyridine) anchors provides an optimal balance between electron injection efficiency and dye stability.[10] In most recent investigations, we have favoured the use of anchoring ligand **1** (Scheme 2); incorporation of an arene spacer between the bpy copper-binding unit and the phosphonic acid functionality improves the photoconversion efficiency of the dye.[11] A 6,6′-substitution pattern is beneficial in stabilizing the copper(I) oxidation state by preventing flattening distortions, and the effects on going from 2,9-dimethyl- to 2,9-bis(trifluoromethyl)- to 2,9-diphenyl-substituted 1,10-phenanthroline in $[Cu(phen)_2]^+$ complexes has been discussed by Armaroli *et al.*[12] Long excited-state lifetimes have been observed as a result of the combined effects of placing bulky substituents in the 2,9- and 3,8-positions of the phen domains in a $[Cu(phen)_2]^+$ photosensitizer.[13] Although Odobel has shown that 6,6′-dimesityl-2,2′-bipyridine-4,4′-dicarboxylic acid is an effective anchor,[4] we have demonstrated that a change from 6,6′-dimethyl substitution pattern in **1** to 6,6′-diphenyl substituents is detrimental to DSC performance.[14,15] We report here the synthesis and application of two new phosphonic acid anchoring ligands (**2** and **3**, Scheme 2) which incorporate 2-thienyl spacers, the advantages of which in dyes are well recognized.[16] Since a combination of **1** with simple halo-functionalized bpy ancillary ligands leads to surprisingly efficient $[Cu(\mathbf{1})(L_{ancillary})]^+$ dyes,[3,17] we chose to use ancillary

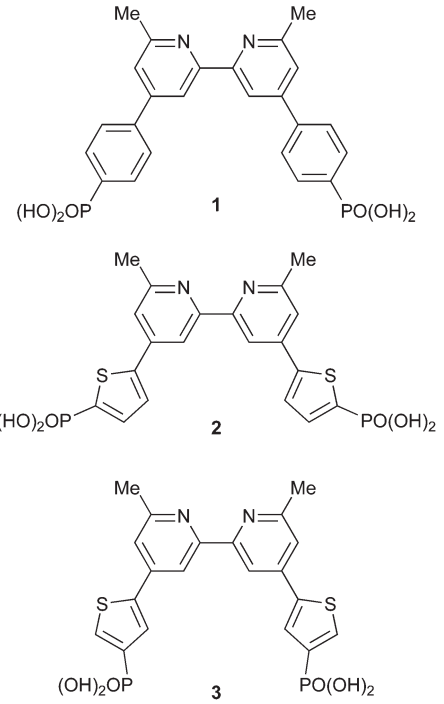

Scheme 2 Structures of anchoring ligands **1–3**.

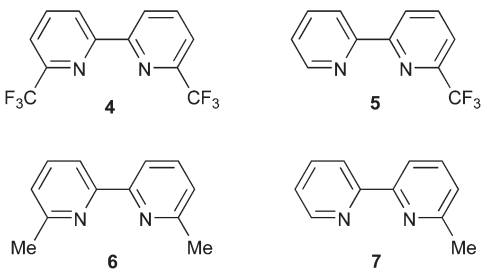

Scheme 3 Structures of ancillary ligands **4–7**.

ligands **4** and **5** (Scheme 3) in a comparative investigation of heteroleptic dyes $[Cu(L_{anchor})(L_{ancillary})]^+$ in which L_{anchor} = **1**, **2** or **3**, and $L_{ancillary}$ = **4–7** (Scheme 3).

Experimental

General

^1H and ^{13}C NMR spectra were recorded on Bruker DRX-500 or 600 NMR spectrometers with chemical shifts referenced to residual solvent peaks (TMS = δ_0 ppm). Electrospray mass spectra and high resolution ESI-MS were measured on Bruker Esquire 3000^{plus} and Bruker maXis 4G instruments, respectively. Solution electronic absorption spectra were recorded on a Agilent 8453 spectrophotometer, and solid-state spectra on a Cary 5000 spectrophotometer. A Biotage Initiator 8 microwave reactor was used for reactions carried out under microwave conditions.

DSC preparation and details of instrumentation for external quantum efficiency and electrochemical impedance spectroscopic measurements are given in the ESI.†

The compounds **1**,[11] $[Cu(\mathbf{4})_2][PF_6]$,[17] $[Cu(\mathbf{5})_2][PF_6]$,[17] $[Cu(\mathbf{6})_2][PF_6]$[18] and $[Cu(\mathbf{7})_2][PF_6]$[8] were prepared as previously reported. The syntheses of precursors are presented in the ESI.†

Compound 2a

4,4′-Bis(5-bromothiophen-2-yl)-6,6′-dimethyl-2,2′-bipyridine (64.8 mg, 0.13 mmol), Cs_2CO_3 (116 mg, 0.36 mmol) and $[Pd(PPh_3)_4]$ (7.4 mg, 0.006 mmol) were added to a microwave vial. The vial was evacuated and flushed with N_2 three times. Then dry THF (5 mL) was added and N_2 was bubbled through the solution for 30 min. Diethyl phosphite (79.0 mg, 0.57 mmol) was added and the N_2 flow continued for 5 min. The reaction mixture was heated in a microwave reactor at 90 °C for 2 h. The resulting mixture was filtered over Celite and the solvent from the filtrate was removed. Compound **2a** was purified by flash column chromatography (SiO_2, cyclohexane/acetone (3/2), R_f: 0.1) and isolated as a pale yellow powder (38 mg, 0.06 mmol, 48%). M.p. 198 °C. ^{1}H NMR (500 MHz, $CDCl_3$) δ/ppm 8.49 (d, J = 1.6 Hz, 2H, H^{A3}), 7.68 (dd, J_{PH} = 8.2 Hz, J_{HH} = 3.7 Hz, 2H, H^{B4}), 7.64 (dd, J_{PH} = 3.6 Hz, J_{HH} = 3.6 Hz, 2H, H^{B3}), 7.39 (d, J = 1.7 Hz, 2H, H^{A5}), 4.28–4.08 (m, 8H, $H^{Et\text{-}CH_2}$), 2.70 (s, 6H, H^{Me}), 1.37 (m, 12H, $H^{Et\text{-}CH_3}$). $^{13}C\{^1H\}$ NMR (126 MHz, $CDCl_3$) δ/ppm 158.1 (C^{A6}), 156.4 (C^{A2}), 149.7 ($C^{A4/B2}$), 141.3 ($C^{A4/B2}$), 137.5 (C^{B4}), 129.0 (d, J_{PC} = 201 Hz, C^{B5}), 126.0 (C^{B3}), 119.8 (C^{A5}), 115.1 (C^{A3}), 62.8 ($C^{Et\text{-}CH_2}$), 24.7 (C^{Me}), 16.2 ($C^{Et\text{-}CH_3}$). $^{31}P\{^1H\}$ NMR (162 MHz, $CDCl_3$) +10.8. ESI-MS m/z 621.1 $[M + H]^+$ (calc. 621.1). High resolution ESI-MS m/z: 621.1407 $[M + H]^+$ (calc. 621.1412). UV-VIS (MeCN, 2.5 × 10^{-5} M) λ/nm (ε/dm^3 mol^{-1} cm^{-1}): 275 (51 600), 299 (59 500). Satisfactory elemental analysis could not be obtained.

Compound 3a

The method was as for **2a** starting with 4,4′-bis(4-bromothiophen-2-yl)-6,6′-dimethyl-2,2′-bipyridine (74.9 mg, 0.15 mmol), Cs_2CO_3 (169 mg, 0.52 mmol), $[Pd(PPh_3)_4]$ (8.6 mg, 0.007 mmol) and diethyl phosphite (81.8 mg, 0.59 mmol). Compound **3a** was obtained as a pale yellow powder (50 mg, 0.08 mmol, 54%). M.p. 188 °C. ^{1}H NMR (500 MHz, $CDCl_3$) δ/ppm 8.50 (br, 2H, H^{A3}), 8.02 (dd, J_{PH} = 8.2 Hz, J_{HH} = 1.2 Hz, 2H, H^{B5}), 7.83 (br. d, 2H, H^{B3}), 7.38 (broadened, 2H, H^{A5}), 4.30–4.01 (m, 8H, $H^{Et\text{-}CH_2}$), 2.72 (s, 6H, H^{Me}), 1.36 (m, 12H, $H^{P\text{-}Me}$). $^{13}C\{^1H\}$ NMR (126 MHz, $CDCl_3$) δ/ppm 158.9 (C^{A6}), 156.1 (C^{A2}), 144.0 ($C^{B2/A4}$), 141.6 ($C^{B2/A4}$) 136.0 (C^{B5}), 131.2 (d, J_{PC} = 197 Hz, C^{B4}), 127.2 (C^{B3}), 119.9 (C^{A5}), 115.2 (C^{A3}), 62.4 (d, J_{PC} = 5.4 Hz, $C^{Et\text{-}CH_2}$), 24.6 (C^{Me}), 16.4 (d, J_{PC} = 6.5 Hz, $C^{Et\text{-}CH_3}$). $^{31}P\{^1H\}$ NMR (202 MHz, $CDCl_3$) +12.0. UV-VIS (MeCN, 2.5 × 10^{-5} M) λ/nm (ε/dm^3 mol^{-1} cm^{-1}): 269 (35 000), 293 (34 500). ESI-MS m/z 621.1 [M + H] (calc. 621.1). Found C 54.44, H 5.89, N 4.40; $C_{28}H_{34}N_2O_6P_2S_2$ requires C 54.19, H 5.52, N 4.51%.

Compound 2

Compound **2a** (20.0 mg, 0.03 mmol) was dissolved in CH_2Cl_2 (5 mL), then Me_3SiBr (98.6 mg, 0.64 mmol) was added and the solution stirred at room temperature overnight. Water (15 mL) was added and the solution stirred for 30 min. A white precipitate formed, was separated by filtration and dried *in vacuo.* Compound **2** (10 mg, 0.02 mmol, 61%) was obtained as an off-white powder. Decomp >275 °C. ^{1}H NMR (600 MHz, DMSO-d_6) δ/ppm 8.41 (s, 2H, H^{A3}), 7.85 (m, 2H, H^{B3}), 7.70 (s, 2H, H^{A5}), 7.50 (dd, J_{PH} = 8.0 Hz, J_{HH} = 3.7 Hz, 2H, H^{B4}), 2.65 (s, 6H, H^{Me}). $^{13}C\{^1H\}$ NMR (151 MHz, DMSO-d_6) δ/ppm 159.4 (C^{A6}), 155.4 (C^{A2}), 146.0 (C^{A4}), 141.7 (C^{B5}), 137.5 (C^{B2}), 135.0 (C^{B4}), 127.2 (C^{B3}), 119.9 (C^{A5}), 114.2 (C^{A3}), 24.7 (C^{Me}). $^{31}P\{^1H\}$ NMR (162 MHz, DMSO-d_6) +4.0. ESI-MS m/z 509.1 $[M + H]^+$ (calc. 509.0). Found C 45.06, H 3.84, N 5.44; $C_{20}H_{18}N_2O_6P_2S_2{\cdot}H_2O$ requires C 45.63, H 3.83, N 5.32%.

Compound 3

The method was as for **2a**, starting with **3a** (60 mg, 0.10 mmol) in CH_2Cl_2 (10 mL) and Me_3SiBr (296 mg, 1.93 mmol). Compound **3** (40 mg, 0.08 mmol, 81%) was isolated as an off-white powder. Decomp >290 °C. ^{1}H NMR (600 MHz, DMSO-d_6) δ/ppm 8.46 (s, 2H, H^{A3}), 8.08 (br. d, J = 8.1 Hz, 2H, H^{B5}), 7.93 (br. m, 2H, H^{B3}), 7.75 (s, 2H, H^{A5}), 2.67 (s, 6H, H^{Me}). $^{13}C\{^1H\}$ NMR (151 MHz, DMSO-d_6) δ/ppm 159.3 (C^{A6}), 142.1 (C^{A4}), 137.9 (C^{B4}), 135.0 (C^{B5}), 128.4 (C^{B3}), 120.3 (C^{A5}), 114.5 (C^{A3}), 24.5 (C^{Me}); C^{A2} and C^{B2} not resolved. $^{31}P\{^1H\}$ NMR (202 MHz, DMSO-d_6) +6.1. ESI-MS m/z 509.1 $[M + H]^+$ (calc. 509.0). Found C 42.08, H 4.37, N 5.17; $C_{20}H_{18}N_2O_6P_2S_2{\cdot}3.5H_2O$ requires C 42.03, H 4.41, N 4.90%.

Crystallography

Data were collected on a Bruker Kappa Apex2 diffractometer with data reduction, solution and refinement using the programs APEX[19] and CRYSTALS.[20] Structural analysis was carried out using Mercury v. 3.5.1.[21,22]

4,4′-Bis(thiophen-2-yl)-6,6′-dimethyl-2,2′-bipyridine

$C_{20}H_{16}N_2S_2$, M = 348.49, light yellow block, monoclinic, space group $P2_1/n$, a = 9.9744(10), b = 4.7410(5), c = 17.6632(17) Å, β = 91.664(4)°, U = 834.92(15) Å^3, Z = 2, D_c = 1.386 Mg m^{-3}, μ(Cu-Kα) = 2.897 mm^{-1}, T = 123 K. Total 9340 reflections, 1509 unique, R_{int} = 0.023. Refinement of 1482 reflections (116 parameters) with $I > 2\sigma(I)$ converged at final R_1 = 0.0487 (R_1 all data = 0.0493), wR_2 = 0.0541 (wR_2 all data = 0.0563), gof = 1.0670. CCDC 1436307.

Compound 2a

$C_{28}H_{34}N_2O_6P_2S_2$, M = 620.67, colourless plate, monoclinic, space group $P2_1/c$, a = 18.3697(12), b = 9.6176(6), c = 8.7340(6) Å, β = 102.202(3)°, U = 1508.20(17) Å^3, Z = 2, D_c = 1.367 Mg m^{-3}, μ(Cu-Kα) = 2.972 mm^{-1}, T = 123 K. Total 11 840 reflections, 2723 unique, R_{int} = 0.036. Refinement of 2268 reflections (181 parameters) with $I > 2\sigma(I)$ converged at final R_1 = 0.0382 (R_1 all data = 0.0473), wR_2 = 0.0931 (wR_2 all data = 0.0988), gof = 0.9296. CCDC 1435291.

Results and discussion

Synthesis of anchoring ligands 2 and 3

The synthesis of anchoring ligands **2** and **3** is based upon our previously published route to ligand **1**.[11] The precursors 4,4′-bis(5-bromothiophen-2-yl)-6,6′-dimethyl-2,2′-bipyridine and 4,4′-bis(4-bromothiophen-2-yl)-6,6′-dimethyl-2,2′-bipyridine were prepared using Kröhnke[23] methodology by treatment of (1*E*,5*E*)-1,6-bis(5-bromothiophen-2-yl)hexa-1,5-diene-3,4-dione or (1*E*,5*E*)-1,6-bis(4-bromothiophen-2-yl)hexa-1,5-diene-3,4-dione with 1-(2-oxopropyl)pyridin-1-ium chloride and NH_4OAc in EtOH (Scheme 4). The compounds were characterized by NMR spectroscopy (Fig. S1 and S2†) and by electrospray mass spectrometry (highest mass peaks at *m*/*z* 506.7 and 506.9, respectively, assigned to $[M + H]^+$). The compounds were then treated with $HPO(OEt)_2$ in the presence of Cs_2CO_3 and $[Pd(PPh_3)_4]$ in THF under microwave conditions to give the phosphonate esters **2a** and **3a** (Scheme 4). The latter were isolated in 48 and 54% yields, respectively. Dehalogenation to give the monoester and 4,4′-bis(thiophen-2-yl)-6,6′-dimethyl-2,2′-bipyridine (Scheme S1†) competed with the formation of the phosphonate esters, as confirmed by spectroscopic data (Fig. S3 and S4†) and the serendipidous growth of single crystals of 4,4′-bis(thiophen-2-yl)-6,6′-dimethyl-2,2′-bipyridine (Fig. S5†). The three products could be readily separated by column chromatography (see Experimental section). Attempts to prepare an analogous compound to **2** and **3** with a phosphonic acid group in the 3-position of the 2-thienyl unit were unsuccessful.

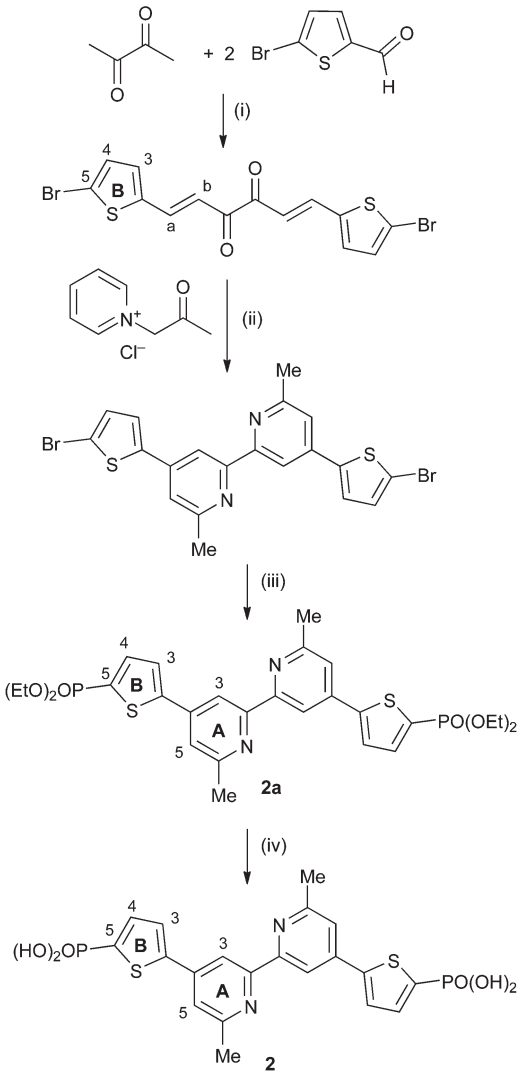

Scheme 4 Synthetic route to compound **2**. Conditions: (i) reflux in MeOH with piperidine, 2 h; (ii) NH_4OAc, EtOH, reflux, 4 h; (iii) Cs_2CO_3, $[Pd(PPh_3)_4]$, $HPO(OEt)_2$ in THF, microwave reactor, 90 °C, 2 h; (iv) Me_3SiBr, CH_2Cl_2. The route to **3** is analogous, with the corresponding diester labelled **3a**.

Esters **2a** and **3a** were converted to phosphonic acids **2** and **3** by treatment with Me_3SiBr,[24] and the products were isolated as white solids in 61 and 81% yields, respectively. The transformation was confirmed in the ^1H and ^{13}C NMR spectra by the disappearance of the signals for the ethyl groups in **2a** and **3a**. Compounds **2a**, **3a**, **2** and **3** were characterized spectroscopically and by mass spectrometry. Elemental analysis for **3a** and **2** were acceptable; acid **3** analysed as the hydrate **3**·3.5H_2O. This is not unreasonable given the presence of two phosphonic acid functionalities, and a singlet at δ 3.43 ppm in the ^1H NMR spectrum of a DMSO-d_6 solution of **2** was observed, consistent with H_2O/HOD. Satisfactory elemental analytical data for **2a** could not be obtained, but composition was confirmed by high resolution electrospray mass spectrometry (*m*/*z*: 620.1407 corresponding to $[M + H]^+$). For each compound, the highest mass peak in the ESI mass spectrum was assigned to $[M + H]^+$ (*m*/*z* 621.1 for **2a** and **3a**, and 509.1 for **2** and **3**). Differing solubilities of **2** and **3** compared to **2a** and **3a** in common solvents meant that the NMR spectra of the acids and esters were recorded in DMSO-d_6 and $CDCl_3$, respectively. On going from **2a** to **2**, and **3a** to **3**, the singlet in the $^{31}P\{^1H\}$ NMR spectrum shifted from δ +10.8 to +4.0 ppm, and from δ +12.0 to +6.1 ppm, respectively. The ^1H and ^{13}C NMR spectra of the compounds were assigned using DEPT, COSY, NOESY, HMQC and HMBC methods (see Experimental section and Scheme 4 for atom labelling). For **3a**, the ^{13}C NMR resonance for C^{A3} (δ 115.2 ppm) could only be located using the HMBC spectrum from the C^{A3}/H^{A5} cross-peak. On going from the bromo-precursor to **2a** (Scheme 4), the singlet in the ^{13}C NMR spectrum for C^{B5} at δ 114.1 ppm is replaced by a doublet (J_{PC} = 201 Hz) at δ 129.0 ppm. Similarly, **3a** exhibited a doublet (J_{PC} = 197 Hz) at δ 131.2 ppm for C^{B4}, in contrast to a singlet at δ 111.2 ppm for C^{B4} in the bromo-precursor. The aromatic regions of the ^1H NMR spectra of phosphonic acids **2** and **3** are shown in Fig. 1. Broadening of the signals is most likely a solvent effect.

Single crystals of **2a** were grown by slowly evaporating an acetone/cyclohexane solution of **2a**. The compound crystallizes in the monoclinic space group $P2_1/c$, and the structure of the centrosymmetric molecule is shown in Fig. 2; selected bond metrics are given in the figure caption and are as expected. The bpy domain is necessarily planar, and the plane of the

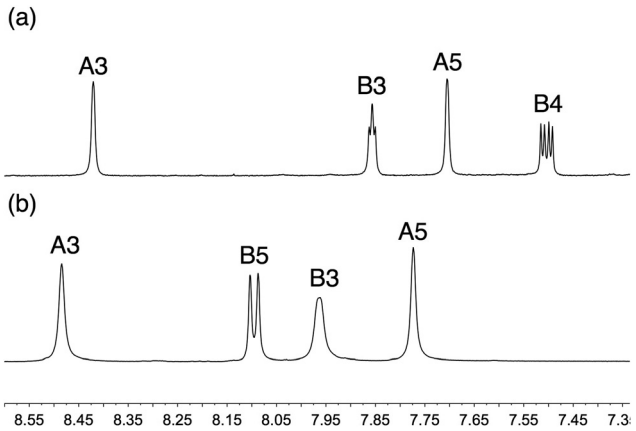

Fig. 1 Aromatic regions of the ^{1}H NMR spectra of (a) **2** and (b) **3** (DMSO-d_6 solutions). Chemical shifts in δ/ppm.

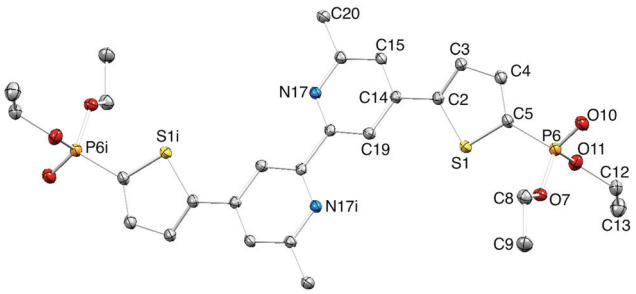

Fig. 2 Structure of **2a**; ellipsoids plotted at 40% probability level and H atoms omitted for clarity. Symmetry code i = 1 − *x*, −*y*, 1 − *z*. Selected bond parameters: S1–C2 = 1.731(2), S1–C5 = 1.718(2), C5–P6 = 1.780(2), P6–O7 = 1.5782(17), P6–O10 = 1.4644(18), P6–O11 = 1.5726(18) Å; C2–S1–C5 = 91.86(11), C5–P6–O7 = 107.07(10), C5–P6–O10 = 112.57(11), O7–P6–O10 = 115.04(10), C5–P6–O11 = 101.27(10), O7–P6–O11 = 101.80(9), O10–P6–O11 = 117.54(10)°.

thienyl unit is twisted 22.2° with respect to the pyridine ring to which it is bonded. The $PO(OEt)_2$ unit is positioned so that the ethoxy groups are above and below the thiophene ring plane, as expected on steric grounds; the O10–P6–C5–C4 torsion angle is 17.3(3)°. The pyridine atom N17 acts as a bifurcated acceptor[25] in C–H···N interactions to a thiophene CH and a methyl CH in adjacent molecules (Fig. 3; $C3^{ii}H31^{ii}\cdots N17$ = 2.54 Å; $C20^{iii}H203^{iii}\cdots N17$ = 2.72 Å; symmetry codes: ii = 1 − *x*, $-\frac{1}{2}+y, \frac{1}{2}-z$; iii = *x*, $\frac{1}{2}-y, \frac{1}{2}+z$). These, along with $C\text{–}H_{ethyl}\cdots O_{PO}$ close contacts, are dominant packing forces are the crystal.

DSC reproducibility and N719 reference DSCs

For the DSC measurements detailed below, duplicate cells for each sensitizer were made and all data are presented to illustrate the reproducibility of the results. All DSCs were fully masked.[26,27] Photoconversion efficiencies are compared with the performance of reference DSCs containing the ruthenium dye N719. Using such relative η values allows valid comparisons between measurements made in different investigations, in different research laboratories, and using different commercial sun simulators (which, in our experience, vary[28]). To validate the reference values, six DSCs containing N719 [1] were assembled (see Experimental section). The reproducibility of plots of current density (J) against potential (V) are confirmed in Fig. S6;† Table S1† gives the performance parameters of the N719 DSCs which show only small variation between devices. In the discussion that follows, average values (Table S1†) of short-circuit current density (J_{SC}), open-circuit voltage (V_{OC}), fill-factor (ff) and photoconversion efficiency (η) for N719 are used.

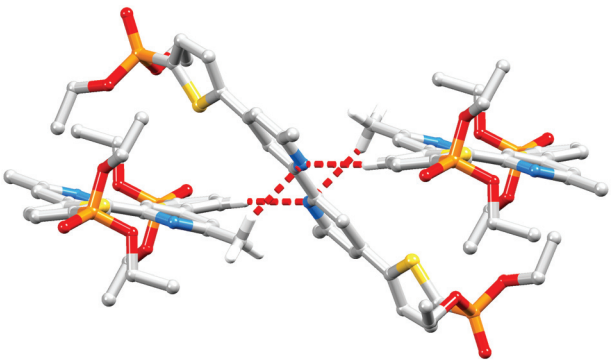

Fig. 3 Bifurcated N···H–C interactions between molecules of **2a**. Hydrogen atoms except for those in the functional groups involved in hydrogen bonding, are omitted for clarity.

Performances of DSCs with dyes with anchor 1: solvent effects

We recently showed that DSCs containing the copper(I) dyes $[Cu(\mathbf{1})(\mathbf{4})]^+$ and $[Cu(\mathbf{1})(\mathbf{5})]^+$ with fluorinated ancillary ligands (Scheme 3) exhibit photoconversion efficiencies of ≈30–34% relative to N719 set at 100%, and outperform DSCs containing $[Cu(\mathbf{1})(\mathbf{6})]^+$ in which **6** contains methyl substituents in the 6- and 6′-positions (Scheme 3).[17] In this study,[17] the exchange reaction (eqn (1)) used to assemble the copper(I) dyes on the TiO_2 electrode was carried out in CH_2Cl_2. Dye-bath solvents are known to influence the performance of DSCs,[29,30] and we attempted to enhance the photoconversion efficiency of dyes $[Cu(\mathbf{1})(\mathbf{4})]^+$ and $[Cu(\mathbf{1})(\mathbf{5})]^+$ by replacing CH_2Cl_2 in the dye-bath by acetone.[29] DSCs were made using commercial TiO_2 electrodes that were sequentially dipped in a dye-bath of a DMSO solution of anchor **1**, and then in a bath containing an acetone solutions of either **4**, **5** or **6** (see Experimental section). The performances and external quantum efficiencies (EQEs) of duplicate DSCs were measured one, three and seven days after fabrication; an I^-/I_3^- electrolyte was used in these solar cells. Values of J_{SC}, V_{OC}, ff and η are given in Table 1. The last column in Table 1 gives values of η relative to N719, for which the relative efficiency is set at 100%. J–V curves and EQE spectra for the DSCs were recorded one day after sealing the cells, and are shown in Fig. 4 and 5.

The data in Table 1 reveal that the DSCs containing $[Cu(\mathbf{1})(\mathbf{4})]^+$ or $[Cu(\mathbf{1})(\mathbf{5})]^+$ significantly outperform those with $[Cu(\mathbf{1})(\mathbf{6})]^+$, as was the case when the dye-bath solvent was CH_2Cl_2. The J–V curves in Fig. 4 show enhancement of both J_{SC} and V_{OC} when

Table 1 Parameters of duplicate, masked DSCs with $[Cu(\mathbf{1})(\mathbf{4})]^+$ and $[Cu(\mathbf{1})(\mathbf{5})]^+$ (fluoro-substituents in $L_{ancillary}$) and $[Cu(\mathbf{1})(\mathbf{6})]^+$ (methyl-substituents) compared to N719; a LOT Quantum Design LS0811 was used as the light source

Dye	J_{SC}/mA cm^{-2}	V_{OC}/mV	ff/%	η/%	Relative η^a/%
1 day after sealing the cells					
$[Cu(\mathbf{1})(\mathbf{4})]^+$	4.58	626	68	1.95	33.6
$[Cu(\mathbf{1})(\mathbf{4})]^+$	4.97	621	67	2.08	35.9
$[Cu(\mathbf{1})(\mathbf{5})]^+$	4.91	613	67	2.03	35.0
$[Cu(\mathbf{1})(\mathbf{5})]^+$	4.34	599	71	1.84	31.7
$[Cu(\mathbf{1})(\mathbf{6})]^+$	3.21	548	69	1.22	21.0
$[Cu(\mathbf{1})(\mathbf{6})]^+$	3.00	551	71	1.17	20.2
N719	13.55	650	66	5.80	100
3 days after sealing the cells					
$[Cu(\mathbf{1})(\mathbf{4})]^+$	4.59	620	70	1.99	33.6
$[Cu(\mathbf{1})(\mathbf{4})]^+$	4.76	614	67	1.97	33.2
$[Cu(\mathbf{1})(\mathbf{5})]^+$	4.81	613	68	2.00	33.7
$[Cu(\mathbf{1})(\mathbf{5})]^+$	4.42	609	73	1.96	33.1
$[Cu(\mathbf{1})(\mathbf{6})]^+$	3.08	540	70	1.17	19.7
$[Cu(\mathbf{1})(\mathbf{6})]^+$	2.90	556	71	1.15	19.4
N719	13.14	684	66	5.93	100
7 days after sealing the cells					
$[Cu(\mathbf{1})(\mathbf{4})]^+$	4.49	610	71	1.96	33.2
$[Cu(\mathbf{1})(\mathbf{4})]^+$	4.81	603	69	2.00	33.9
$[Cu(\mathbf{1})(\mathbf{5})]^+$	4.74	614	68	1.98	33.6
$[Cu(\mathbf{1})(\mathbf{5})]^+$	4.48	611	73	2.00	33.9
$[Cu(\mathbf{1})(\mathbf{6})]^+$	3.04	537	70	1.15	19.5
$[Cu(\mathbf{1})(\mathbf{6})]^+$	2.82	564	70	1.12	19.0
N719	13.05	691	66	5.90	100

[a] Relative to N719 set at 100%. See Table S1 for N719 DSCs.

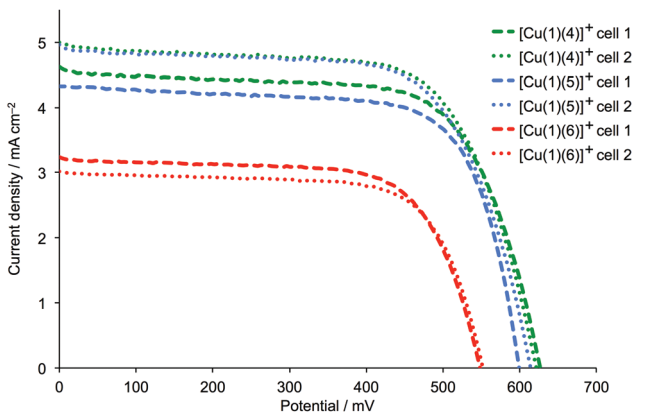

Fig. 4 *J–V* curves for duplicate DSCs with $[Cu(\mathbf{1})(\mathbf{4})]^+$, $[Cu(\mathbf{1})(\mathbf{5})]^+$ and $[Cu(\mathbf{1})(\mathbf{6})]^+$, recorded one day after DSC fabrication.

CF_3 groups are introduced into the ancillary ligand. Good fill-factors of ~70% are achieved for all DSCs, and the global efficiencies are maintained over a week after sealing the cells. The longer-term stability of a DSC containing $[Cu(\mathbf{1})(\mathbf{5})]^+$ was confirmed with values of J_{SC} = 4.48 mA cm^{-2}, V_{OC} = 603 mV, ff = 70% and η = 1.90% recorded after 50 days. The EQE spectra of the DSCs are shown in Fig. 5 and are consistent with the improved J_{SC} values of $[Cu(\mathbf{1})(\mathbf{4})]^+$ or $[Cu(\mathbf{1})(\mathbf{5})]^+$ *versus* $[Cu(\mathbf{1})(\mathbf{6})]^+$ (Table 1). For the DSCs in which the sensitizer is $[Cu(\mathbf{1})(\mathbf{4})]^+$ or $[Cu(\mathbf{1})(\mathbf{5})]^+$, EQE_{max} lies between 44.1% and 49.6% (λ_{max} = 470–480 nm). This considerably exceeds values of EQE_{max} = 33.5–35.5% (λ_{max} = 480 nm) for the DSCs containing $[Cu(\mathbf{1})(\mathbf{6})]^+$. Inclusion of fluoro-substituted ancillary ligands **4** or **5** leads to relative photoconversion efficiencies of ~33% after 3 to 7 days (with respect to 100% for N719). This is similar to the relative values of η obtained for DSCs assembled using CH_2Cl_2 in the dye-bath[17] and we conclude that in this case, the choice of CH_2Cl_2 or acetone has no significant impact on the DSC performance.

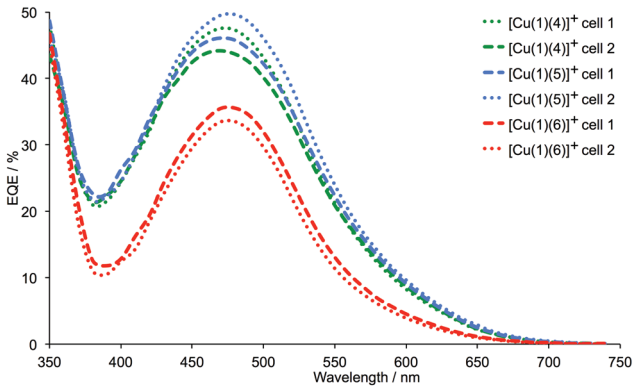

Fig. 5 EQE spectra for duplicate DSCs with $[Cu(\mathbf{1})(\mathbf{4})]^+$, $[Cu(\mathbf{1})(\mathbf{5})]^+$ and $[Cu(\mathbf{1})(\mathbf{6})]^+$, recorded one day after DSC fabrication.

Although the sealed DSCs are stable, both acetone and CH_2Cl_2 solutions of $[Cu(\mathbf{4})_2][PF_6]$ lose their orange colour within a week. For this reason, we initially focused attention on the use of **5** for DSC investigations with the anchors **2** and **3**.

DSCs with $[Cu(L_{anchor})(\mathbf{5})]^+$ dyes with L_{anchor} = 1, 2 or 3

The heteroleptic dyes $[Cu(\mathbf{1})(\mathbf{5})]^+$, $[Cu(\mathbf{2})(\mathbf{5})]^+$ and $[Cu(\mathbf{3})(\mathbf{5})]^+$ were assembled on commercial FTO/TiO_2 electrodes with and without scattering layers. The latter were used to record solid-state absorption spectra and the former to fabricate DSCs (see Experimental section). Solid-state absorption spectra of the adsorbed dyes $[Cu(\mathbf{1})(\mathbf{5})]^+$, $[Cu(\mathbf{2})(\mathbf{5})]^+$ and $[Cu(\mathbf{3})(\mathbf{5})]^+$ are shown in Fig. 6. A small red-shift in λ_{max} is observed on going from

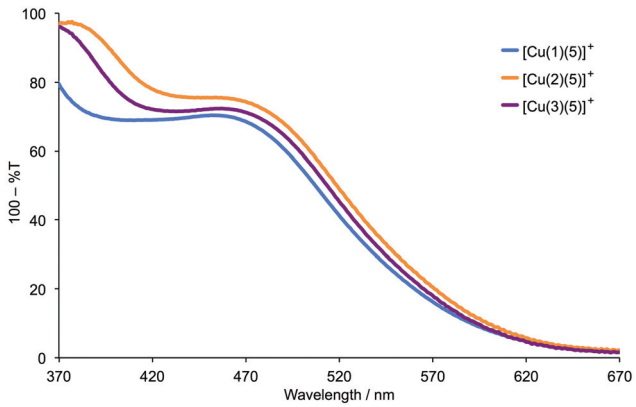

Fig. 6 Solid-state absorption spectra of FTO/TiO_2 electrodes with adsorbed dyes $[Cu(\mathbf{1})(\mathbf{5})]^+$, $[Cu(\mathbf{2})(\mathbf{5})]^+$ and $[Cu(\mathbf{3})(\mathbf{5})]^+$. The spectra were recorded in transmission mode, and data are presented as 100% T for ease of interpretation of λ_{max}.

$[Cu(\mathbf{1})(\mathbf{5})]^+$ (460 nm) to $[Cu(\mathbf{2})(\mathbf{5})]^+$ and $[Cu(\mathbf{3})(\mathbf{5})]^+$ (470 nm), and the absorption band is broadened towards the red-end of the spectrum.

Performance data for the DSCs over a period of a week are given in Table 2, and there is satisfactory reproducibility between the performances of pairs of cells containing the same dye. Fig. 7 shows the *J*–*V* curves for the DSCs on the day of cell assembly. Replacement of the phenyl spacer in anchor **1** by a 2-thienyl spacer in **2** and **3** results in an increase in the short-circuit current density, and this is most noticeable for the sensitizer $[Cu(\mathbf{3})(\mathbf{5})]^+$. Fig. 7 and Table 2 illustrate that values of V_{OC} for DSCs with $[Cu(\mathbf{1})(\mathbf{5})]^+$ and $[Cu(\mathbf{3})(\mathbf{5})]^+$ are essentially the same, whereas devices with $[Cu(\mathbf{2})(\mathbf{5})]^+$ consistently exhibit lower values of V_{OC}. Within experimental error, the global efficiencies of the DSCs are stable over time, and Table 2 shows that the best performing dye is that containing anchor **3**, *i.e.* the 2-thienyl spacer with phosphonic acid in the 4-position (Scheme 2). The EQE spectra in Fig. 8 (see also Table 3) are consistent with the enhanced J_{SC} values for $[Cu(\mathbf{2})(\mathbf{5})]^+$ and $[Cu(\mathbf{3})(\mathbf{5})]^+$. The values of EQE_{max} of 52.9 and 51.8% (Table 3) for the duplicate DSCs with $[Cu(\mathbf{3})(\mathbf{5})]^+$ coupled with the enhanced quantum efficiences towards the red-end of the spectrum compared to the EQE spectra for the DSCs containing $[Cu(\mathbf{1})(\mathbf{5})]^+$ (Fig. 8) are noteworthy. The EQE spectra of DSCs with $[Cu(\mathbf{2})(\mathbf{5})]^+$ (Fig. 8) also show a broad spectral response.

To further validate the improvement in V_{OC} on going from **2** to **3**, we repeated the DSC performance measurements using in-house, screen-printed FTO/TiO_2 electrodes. The dyes

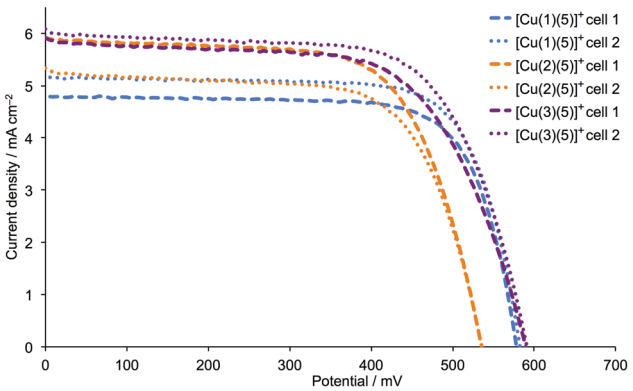

Fig. 7 *J*–*V* curves for duplicate DSCs with $[Cu(\mathbf{1})(\mathbf{5})]^+$, $[Cu(\mathbf{2})(\mathbf{5})]^+$ and $[Cu(\mathbf{3})(\mathbf{5})]^+$ and commercial FTO/TiO_2 electrodes, recorded on the day of DSC fabrication.

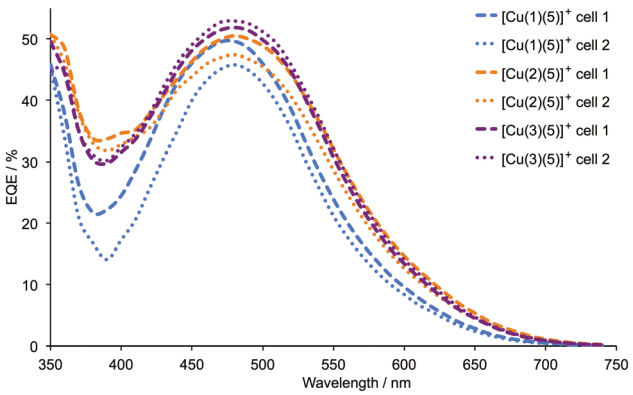

Fig. 8 EQE spectra for duplicate DSCs with $[Cu(\mathbf{1})(\mathbf{5})]^+$, $[Cu(\mathbf{2})(\mathbf{5})]^+$ and $[Cu(\mathbf{3})(\mathbf{5})]^+$ and commercial FTO/TiO_2 electrodes, recorded on the day of DSC assembly.

Table 2 Parameters of duplicate, masked DSCs with $[Cu(\mathbf{1})(\mathbf{5})]^+$, $[Cu(\mathbf{2})(\mathbf{5})]^+$ and $[Cu(\mathbf{3})(\mathbf{5})]^+$ compared to N719; commercial electrodes were used for the photoanodes; a LOT Quantum Design LS0811 was used as the light source

Dye	J_{SC}/mA cm^{-2}	V_{OC}/mV	ff/%	η/%	Relative η^a/%
On the day of sealing the cells					
$[Cu(\mathbf{1})(\mathbf{5})]^+$	5.45	606	69	2.26	39.2
$[Cu(\mathbf{1})(\mathbf{5})]^+$	5.16	582	74	2.22	38.5
$[Cu(\mathbf{2})(\mathbf{5})]^+$	5.90	535	67	2.13	37.0
$[Cu(\mathbf{2})(\mathbf{5})]^+$	5.28	535	68	1.91	33.2
$[Cu(\mathbf{3})(\mathbf{5})]^+$	5.87	589	64	2.23	38.7
$[Cu(\mathbf{3})(\mathbf{5})]^+$	6.02	591	67	2.40	41.7
N719	13.64	636	66	5.76	100
3 days after sealing the cells					
$[Cu(\mathbf{1})(\mathbf{5})]^+$	4.81	613	68	2.00	33.7
$[Cu(\mathbf{1})(\mathbf{5})]^+$	4.42	609	73	1.96	33.1
$[Cu(\mathbf{2})(\mathbf{5})]^+$	5.46	552	64	1.93	32.5
$[Cu(\mathbf{2})(\mathbf{5})]^+$	4.98	557	67	1.86	31.4
$[Cu(\mathbf{3})(\mathbf{5})]^+$	5.25	611	65	2.08	35.1
$[Cu(\mathbf{3})(\mathbf{5})]^+$	5.66	600	67	2.29	38.6
N719	13.14	684	66	5.93	100
7 days after sealing the cells					
$[Cu(\mathbf{1})(\mathbf{5})]^+$	4.74	614	68	1.98	33.6
$[Cu(\mathbf{1})(\mathbf{5})]^+$	4.48	611	73	2.00	33.9
$[Cu(\mathbf{2})(\mathbf{5})]^+$	5.43	566	68	2.09	35.4
$[Cu(\mathbf{2})(\mathbf{5})]^+$	4.93	564	68	1.90	32.2
$[Cu(\mathbf{3})(\mathbf{5})]^+$	5.10	619	67	2.10	35.6
$[Cu(\mathbf{3})(\mathbf{5})]^+$	5.42	601	69	2.25	38.1
N719	13.05	691	66	5.90	100

[a] Relative to N719 set at 100%. See Table S1 for N719 DSCs.

Table 3 EQE maxima for DSCs containing $[Cu(\mathbf{1})(\mathbf{5})]^+$, $[Cu(\mathbf{2})(\mathbf{5})]^+$ and $[Cu(\mathbf{3})(\mathbf{5})]^+$ (commercial electrodes) measured on the day of cell assembly

	Cell 1		Cell 2	
Anchored dye	λ_{max}/nm	EQE_{max}/%	λ_{max}/nm	EQE_{max}/%
$[Cu(\mathbf{1})(\mathbf{5})]^+$	480	45.8	480	49.6
$[Cu(\mathbf{2})(\mathbf{5})]^+$	480	46.4	480	46.0
$[Cu(\mathbf{3})(\mathbf{5})]^+$	480	44.1	480	46.9

$[Cu(\mathbf{2})(\mathbf{5})]^+$ and $[Cu(\mathbf{3})(\mathbf{5})]^+$ were assembled on the electrodes by the step-wise approach shown in eqn (1); the photoanodes were incorporated into DSCs along with I^-/I_3^- electrolyte. DSC performance parameters are given in Table S2,† and Fig. 9 shows the respective *J*–*V* curves. The ~55–60 mV gain in V_{OC} mirrors that seen when commercial electrodes were used (Fig. 7 *vs.* Fig. 9), and values of J_{SC} are similar. EQE spectra (Fig. S7†) all show EQE_{max} > 50% (Table 4) and the same extension of the spectral response to higher wavelengths. Thus, data

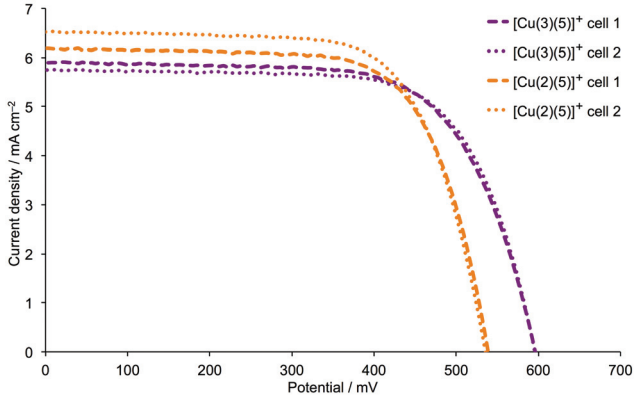

Fig. 9 *J–V* curves for duplicate DSCs with $[Cu(\mathbf{2})(\mathbf{5})]^+$ and $[Cu(\mathbf{3})(\mathbf{5})]^+$ dyes on in-house screen-printed FTO/TiO_2 electrodes, recorded on the day of DSC assembly.

Table 4 EQE maxima for duplicate DSCs containing dyes $[Cu(\mathbf{1})(\mathbf{5})]^+$, $[Cu(\mathbf{2})(\mathbf{5})]^+$ and $[Cu(\mathbf{3})(\mathbf{5})]^+$ and in-house screen-printed electrodes, measured on the day of cell assembly

	Cell 1		Cell 2	
Anchored dye	λ_{max}/nm	EQE_{max}/%	λ_{max}/nm	EQE_{max}/%
$[Cu(\mathbf{2})(\mathbf{5})]^+$	480	55.2	480	53.0
$[Cu(\mathbf{3})(\mathbf{5})]^+$	480	55.8	480	53.9

for DSCs made using self-printed FTO/TiO_2 electrodes confirm that higher V_{OC} values are achieved if the phosphonic acid anchor-groups are located in the 4- rather than 5-positions of the thienyl functionality.

The longer-term stability of DSCs containing $[Cu(\mathbf{2})(\mathbf{5})]^+$ and $[Cu(\mathbf{3})(\mathbf{5})]^+$ (both with commercial and in-house screen-printed electrodes) was assessed by measurements made after 41 or 46 days. A comparison of the data in Table 5 with the characteristics of 7-day old DSCs containing $[Cu(\mathbf{2})(\mathbf{5})]^+$ and $[Cu(\mathbf{3})(\mathbf{5})]^+$ (Tables 2 and S2†) confirm little change in J_{SC}, V_{OC} and η values for a given DSC over a 6-week period.

Table 5 Long-term stability tests of duplicate, masked DSCs containing $[Cu(\mathbf{2})(\mathbf{5})]^+$ and $[Cu(\mathbf{3})(\mathbf{5})]^+$; a LOT Quantum Design LS0811 was used as the light source. Compare data with those in Tables 2 and S2

Dye	Age of DSC/days	J_{SC}/mA cm^{-2}	V_{OC}/mV	ff/%	η/%
Commercial FTO/TiO_2 electrodes					
$[Cu(\mathbf{2})(\mathbf{5})]^+$	46	5.23	572	70	2.10
$[Cu(\mathbf{2})(\mathbf{5})]^+$	46	4.70	568	71	1.90
$[Cu(\mathbf{3})(\mathbf{5})]^+$	46	5.08	615	69	2.15
$[Cu(\mathbf{3})(\mathbf{5})]^+$	46	5.07	613	72	2.22
In-house, screen-printed FTO/TiO_2 electrodes					
$[Cu(\mathbf{2})(\mathbf{5})]^+$	41	5.65	549	70	2.17
$[Cu(\mathbf{2})(\mathbf{5})]^+$	41	5.82	545	69	2.19
$[Cu(\mathbf{3})(\mathbf{5})]^+$	41	5.39	625	69	2.32
$[Cu(\mathbf{3})(\mathbf{5})]^+$	41	5.41	616	70	2.34

Combining thienyl-spaced anchors with different ancillary ligands

We have now shown that although comparable DSC performances are achieved using either a 2-thienyl or phenyl spacer in the phosphonic acid anchoring ligand, higher V_{OC} values result if the phosphonic acid group is in the 4- rather than 5-position of the thienyl ring. This conclusion was reached using a single ancillary ligand, **5**. To validate the conclusions, we extended the study to dyes containing combinations of **1**, **2** and **3** with ancillary ligands **6** and **7** (Scheme 3).

Tables 6 and S3† present performance parameters for pairs of DSCs containing $[Cu(L_{anchor})(L_{ancillary})]^+$ with L_{anchor} = **1–3** and $L_{ancillary}$ = **6**, **7**. *J–V* curves for one set of DSCs with each ancillary ligand are shown in Fig. 10; Fig. S8† gives a compari-

Table 6 Parameters of duplicate, masked DSCs with $[Cu(L_{anchor})(L_{ancillary})]^+$ (L_{anchor} = **1–3**, $L_{ancillary}$ = **6**, **7**) compared to a reference DSC with N719; commercial FTO/TiO_2 electrodes were used. The light source was a LOT Quantum Design LS0811. See also Table S3

Dye	J_{SC}/mA cm^{-2}	V_{OC}/mV	ff/%	η/%	Relative η^a/%
On the day of sealing the cells					
$[Cu(\mathbf{1})(\mathbf{6})]^+$	4.19	554	69	1.60	27.8
$[Cu(\mathbf{1})(\mathbf{6})]^+$	3.78	550	69	1.44	25.0
$[Cu(\mathbf{1})(\mathbf{7})]^+$	3.78	552	75	1.56	27.1
$[Cu(\mathbf{1})(\mathbf{7})]^+$	4.58	551	72	1.83	31.8
$[Cu(\mathbf{2})(\mathbf{6})]^+$	4.08	511	74	1.54	26.7
$[Cu(\mathbf{2})(\mathbf{6})]^+$	4.33	509	73	1.61	28.0
$[Cu(\mathbf{2})(\mathbf{7})]^+$	4.96	527	73	1.91	33.2
$[Cu(\mathbf{2})(\mathbf{7})]^+$	5.35	521	74	2.07	35.9
$[Cu(\mathbf{3})(\mathbf{6})]^+$	4.17	544	72	1.64	28.5
$[Cu(\mathbf{3})(\mathbf{6})]^+$	3.85	532	72	1.48	25.7
$[Cu(\mathbf{3})(\mathbf{7})]^+$	4.69	562	70	1.85	32.1
$[Cu(\mathbf{3})(\mathbf{7})]^+$	5.22	565	72	2.13	37.0
N719	13.64	636	66	5.76	100

[a] Relative to N719 set at 100%.

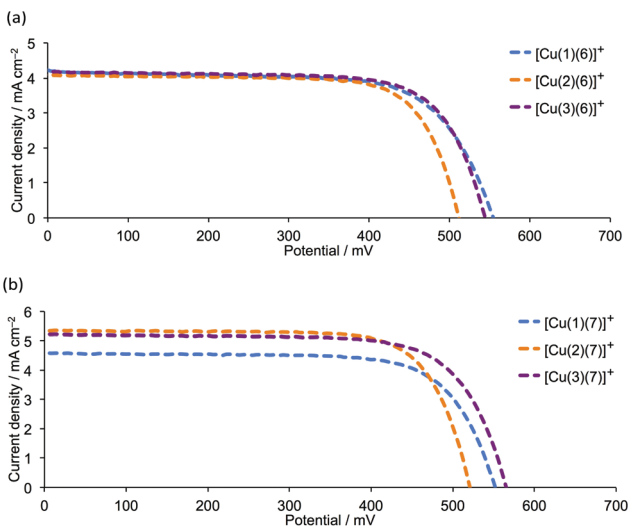

Fig. 10 *J–V* curves for DSCs with (a) $[Cu(L_{anchor})(\mathbf{6})]^+$ and (b) $[Cu(L_{anchor})(\mathbf{7})]^+$ dyes (L_{anchor} = **1**, **2** and **3**) on commercial FTO/TiO_2 electrodes, recorded on the day of DSC assembly. See also Fig. S8.†

son of *J*–*V* curves for duplicate DSCs containing ancillary ligand **6**. Pleasingly, the same trend observed in the series [Cu(**1**)(**5**)]$^+$, [Cu(**2**)(**5**)]$^+$ and [Cu(**3**)(**5**)]$^+$ (Fig. 7 and 9) is followed by [Cu(**1**)(**6**)]$^+$, [Cu(**2**)(**6**)]$^+$ and [Cu(**3**)(**6**)]$^+$ (Fig. 10a) and by [Cu(**1**)(**7**)]$^+$, [Cu(**2**)(**7**)]$^+$ and [Cu(**3**)(**7**)]$^+$ (Fig. 10b). Both the anchors with the thienyl spacer perform well, but a significant gain in V_{OC} (~40 to 50 mV) is achieved on going from anchor **2** to **3**. On the day of DSC assembly (Table 6), values of J_{SC} are similar for [Cu(**1**)(**6**)]$^+$, [Cu(**2**)(**6**)]$^+$ and [Cu(**3**)(**6**)]$^+$ (Fig. 10a) and are somewhat higher for [Cu(**2**)(**7**)]$^+$ and [Cu(**3**)(**7**)]$^+$ with respect to [Cu(**1**)(**7**)]$^+$ (Fig. 10b). The origin of this improvement in J_{SC} is nicely illustrated by the EQE spectra shown in Fig. 11, with enhanced quantum efficiencies above ~530 nm being consistent with the discussion of the EQE spectra of [Cu(**2**)(**5**)]$^+$ and [Cu(**3**)(**5**)]$^+$ (Fig. 8). On going from [Cu(**1**)(**7**)]$^+$ to [Cu(**2**)(**7**)]$^+$ and [Cu(**3**)(**7**)]$^+$, the value of λ_{max} corresponding to EQE_{max} undergoes a red-shift of 10 nm (Fig. 11 and Table 7). For $L_{ancillary}$ = **6** or **7**, the global efficiencies of 7-day old DSCs (Table S3†) containing anchors **2** or **3** are slightly improved with respect to those with anchor **1**. Fig. 12 summarizes the photoconversion efficiencies of DSCs with different $L_{anchor}/L_{ancillary}$ combinations, and illustrates clearly that **3** is the best of the anchoring ligands, and **5** is the leading ancillary ligand.

One *versus* two methyl groups, and a methyl *versus* trifluoromethyl group in $L_{ancillary}$

In this section, we comment briefly on the comparison of one or two methyl substituents in the ancillary ligand, and compare the performances of DSCs with [Cu(L_{anchor})(**7**)]$^+$ and [Cu(L_{anchor})(**5**)]$^+$ (**5** and **7** differ in bearing either a CF_3 or CH_3 group in the 6-position of the bpy unit).

In previous investigations, we have shown that the incorporation of methyl substituents in the 6- and 6′-positions of a bpy-based ancillary ligand improves DSC performance.[7,14] The data in Table 6 for pairs of sensitizers [Cu(L_{anchor})(**6**)]$^+$ and [Cu(L_{anchor})(**7**)]$^+$ illustrate enhanced DSC performance on going from an ancillary ligand with a 6,6′-dimethyl substitution to one with a single 6-methyl group (an observation that is supported by the EIS measurments discussed later). In all dyes, the anchoring ligand contains a 6,6′-dimethyl-2,2′-bipyridine core. The improvement is most noticable for dyes with anchors **2** and **3**, and has its origins in increased values of both J_{SC} and V_{OC}.

The data in Table 2, Fig. 7 and 8 illustrate how the performances of DSCs with the dyes [Cu(L_{anchor})(**5**)]$^+$ vary as a function of L_{anchor}. Analogous information for the series of [Cu(L_{anchor})(**7**)]$^+$ dyes is presented in Table 6, Fig. 10 and 11. A comparison of the two sets of results confirms that the replacement of a 6-methyl substituent in **7** by a trifluoromethyl group in **5** leads to an enhancement in photoconversion efficiency. On going from [Cu(**1**)(**7**)]$^+$ to [Cu(**1**)(**5**)]$^+$, J_{SC} increases from 4.58 to 5.45 mA cm^{-2} (best values are selected from duplicate DSCs) on the day the DSCs were sealed, and the difference is maintained after a week (3.79 *versus* 4.74 mA cm^{-2}). Enhanced V_{OC} is also observed on the initial day (551 to 582 mV), with this differentiation retained as the DSCs age. For DSCs containing [Cu(**3**)(**7**)]$^+$ or [Cu(**3**)(**5**)]$^+$, there is a notable improvement in J_{SC} on introducing the fluoro-substituents. For 7-day old DSCs, values of J_{SC} = 4.13 and 4.44 mA cm^{-2} for [Cu(**3**)(**7**)]$^+$ (Table 6) increase to 5.10 and 5.42 mA cm^{-2} for [Cu(**3**)(**5**)]$^+$ (Table 2), and the global efficiencies increase from 1.77 and 1.96% for duplicate DSCs to 2.10 and 2.25% (compared to 5.90% for N719). The trends substantiate those previously reported,[17] and in order to gain a better understanding of the contributing factors, we have applied the method of electrochemical impedance spectroscopy.

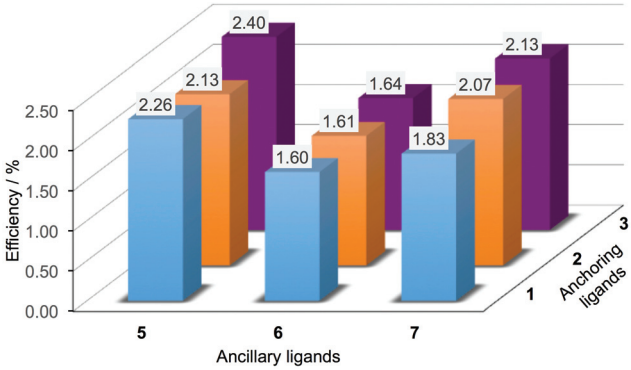

Fig. 12 Best photoconversion efficiencies, η, of DSCs containing [Cu(L_{anchor})($L_{ancillary}$)]$^+$ sesnitizers with L_{anchor} = **1–3** and $L_{ancillary}$ = **5–7**. Measurements were made on the day of DSC fabrication and N719 achieves a value of η = 5.76% under the same conditions.

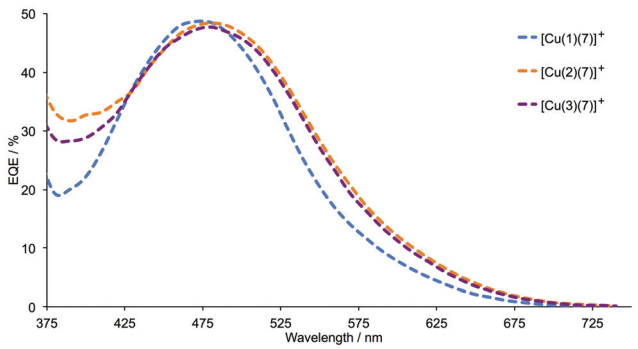

Fig. 11 EQE spectra for DSCs with [Cu(L_{anchor})(**7**)]$^+$ (L_{anchor} = **1**, **2** and **3**) on commercial FTO/TiO_2 electrodes, recorded on the day of assembling the DSCs.

Table 7 EQE maxima for duplicate DSCs containing [Cu(L_{anchor})(**7**)]$^+$ with L_{anchor} = **1–3** and using commercial electrodes; the spectra were recorded on the day of cell assembly

	Cell 1		Cell 2	
Anchored dye	λ_{max}/nm	EQE_{max}/%	λ_{max}/nm	EQE_{max}/%
[Cu(**1**)(**7**)]$^+$	470	48.6	470	41.5
[Cu(**2**)(**7**)]$^+$	480	48.4	480	46.1
[Cu(**3**)(**7**)]$^+$	480	47.7	480	45.4

Electrochemical impedance spectroscopy: introductory comments

EIS is a powerful tool for the analysis and evaluation of the performance and properties of electrochemical systems and is highly suited to investigations of charge transfer processes in DSCs.[31,32] A small alternating current (AC) of varying frequency is applied close to the open-circuit potential of the DSC which may be placed under a bias-light of different intensities.[33] The internal impedances at the various frequencies correspond to different processes in the cell. The results are commonly plotted in a Nyquist plot (Fig. 13) where each semi-circle in the plot provides information about the charge-transfer resistances and capacitances of the corresponding interface in a DSC.[34] Recombination reactions or 'back reactions' are the main limiting factors affecting the photoconversion efficiency of a DSC.[35]

From the parameters extracted from EIS data, the length of the electron diffusion, L_d, and the electron lifetime (τ) in the semiconductor (SC), can be obtained.[36] These are given by eqn (2) and (3), respectively, where R_t is the transport resistance in the SC, C_μ is the chemical capacitance of the TiO_2/electrolyte interface (with the capacitance of the transparent conductive oxide layer/electrolyte neglected at higher bias voltages when the SC is conducting) and L is the thickness of the porous active layer.

$$L_d = L\sqrt{\frac{R_{rec}}{R_t}} \quad (2)$$

$$\tau = R_{rec}C_\mu \quad (3)$$

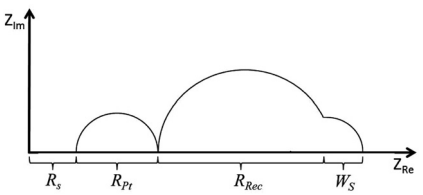

Fig. 13 Schematic representation of a Nyquist plot. R_s is the electrical resistance in cables, contacts and the resistance of the semi-conductor/FTO glass. R_{Pt} is the charge transfer resistance of the interface cathode/electrolyte. R_{rec} is the electron recombination resistance of the active layer/electrolyte and W_s is the Warburg short resistance of the ion diffusion in the electrolyte close to the active layer surface.

Studies of R_t are best carried out at lower bias-light intensities, since at higher open-circuit voltages, the SC exhibits electron-transport properties closer to that of a conductor; thus, R_t becomes lower and more difficult to observe. At a given illumination intensity (given that the geometry of the electrode is constant), it can be assumed that the Fermi level (E_F) and the resistance of TiO_2 (R_0) are constant. From eqn (4) it then follows that a change of the lower level of the conduction band (E_{cb}) is the one main parameter that will affect R_t on the surface, close to the dye/electrolyte.[37]

$$R_t = R_0 \exp\left[-\frac{E_F - E_{cb}}{kT}\right] \quad (4)$$

The electrolyte composition and the dye are factors that influence the values of E_{cb} and therefore V_{OC}.[37] In a well-performing DSC, the recombination resistance should be significantly higher than the transport resistance. In this case, electrons injected into the TiO_2 are readily collected, and the tendency to recombine with the oxidized dye or the oxidized form of the electrolyte is suppressed. It follows from eqn (2) that the normalized diffusion length L_d/L will be greater than unity.[36] The physical meaning is that L_d for the injected electron to reach the p–n junction and combine with the generated hole should be at least longer than L.

EIS measurements: DSCs with dyes with anchor 1

We initially focus on EIS data for 3-day old DSCs containing the dyes $[Cu(\mathbf{1})(\mathbf{4})]^+$, $[Cu(\mathbf{1})(\mathbf{5})]^+$, $[Cu(\mathbf{1})(\mathbf{6})]^+$ and $[Cu(\mathbf{1})(\mathbf{7})]^+$ with the phenyl-spacer in the anchoring ligand. As discussed earlier, DSC performance parameters showed that dyes containing CF_3 groups in the ancillary ligand exhibit higher V_{OC} values than the CH_3 analogues. This trend is confirmed by the V_{OC} values determined at different light intensities from EIS measurements. Table S4† presents all data, and Tables 8 and 9 give data at the lowest and highest light intensities measured; Nyquist and Bode plots are shown in Table S5.† A higher V_{OC} implies that more electrons are present in the conduction band of the SC, which indicates a more negative conduction band level (E_{cb}). This is supported by the values of R_t given in Table 9 (where EIS data are from measurements at lower bias-light intensities). The values of R_t are significantly lower for dyes containing **4** and **5** than **6** and **7**. On the other hand, the DSCs containing $[Cu(\mathbf{1})(\mathbf{6})]^+$ or $[Cu(\mathbf{1})(\mathbf{7})]^+$ exhibit higher R_{rec}

Table 8 Impedance data obtained during measurements at 22 mW cm^{-2}. EIS measurements are carried out 3 days after DSC assembly

	R_s/Ω	R_{rec}/Ω	C_μ/μF	R_{Pt}/Ω	C_{Pt}/μF	τ/ms	V_{OC}/mV	η^a/%
$[Cu(\mathbf{1})(\mathbf{4})]^+$	14.9	172.0	251.8	49.4	5.4	43.3	630	1.97
$[Cu(\mathbf{1})(\mathbf{5})]^+$	12.2	204.3	276.1	47.4	5.2	56.4	620	2.00
$[Cu(\mathbf{1})(\mathbf{6})]^+$	9.3	316.0	183.3	53.3	4.7	57.9	530	1.15
$[Cu(\mathbf{1})(\mathbf{7})]^+$	15.4	250.5	201.4	14.2	4.6	50.4	553	1.53
$[Cu(\mathbf{2})(\mathbf{5})]^+$	13.7	94.1	197.0	54.5	4.8	18.5	582	1.93
$[Cu(\mathbf{3})(\mathbf{5})]^+$	18.6	150.8	309.1	31.7	4.7	46.6	594	2.29
$[Cu(\mathbf{2})(\mathbf{7})]^+$	12.3	107.2	222.6	9.8	5.2	23.9	578	1.89
$[Cu(\mathbf{3})(\mathbf{7})]^+$	10.6	136.2	320.3	13.0	4.3	43.6	622	1.97

[a] The cell efficiency is that of the particular cell measured with EIS.

Table 9 Impedance data obtained during measurements at 2.4 mW cm^{-2}. EIS measurements are carried out 3 days after DSC assembly

	R_s/Ω	R_t/Ω	R_{rec}/Ω	C_μ/μF	R_{Pt}/Ω	C_{Pt}/μF	τ/ms	L_d/L (dimensionless)	V_{OC}/mV
[Cu(**1**)(**4**)]$^+$	14.9	192.8	1068.0	131.0	59.0	4.8	139.9	2.4	550
[Cu(**1**)(**5**)]$^+$	11.7	104.3	1242.0	158.5	52.8	4.7	196.9	3.5	550
[Cu(**1**)(**6**)]$^+$	7.0	288.6	2420.0	88.3	91.2	6.9	213.6	2.9	440
[Cu(**1**)(**7**)]$^+$	13.0	228.0	1723.0	130.1	16.0	8.6	224.1	2.7	493
[Cu(**2**)(**5**)]$^+$	12.3	251.2	738.0	93.2	59.0	5.8	68.8	1.7	510
[Cu(**3**)(**5**)]$^+$	16.4	67.8	917.4	182.0	35.3	4.4	166.9	3.7	520
[Cu(**2**)(**7**)]$^+$	11.6	203.3	787.1	109.0	13.2	8.8	85.8	2.0	516
[Cu(**3**)(**7**)]$^+$	10.6	44.1	999.3	178.0	14.8	3.9	177.9	4.8	539

values (Fig. 14a and 15). However, the electron lifetimes (plotted in Fig. 14b *versus* the bias-light intensity) for DSCs with [Cu(**1**)(**4**)]$^+$, [Cu(**1**)(**5**)]$^+$, [Cu(**1**)(**6**)]$^+$, [Cu(**1**)(**7**)]$^+$ are in the same range. The electron lifetime is the product of R_{rec} and C_μ, and it therefore follows that the capacitance must be significantly larger for the trifluoromethylated dyes [Cu(**1**)(**4**)]$^+$ and [Cu(**1**)(**5**)]$^+$, as confirmed in Fig. 16. Inspection of Tables 8 and 9 reveals that the DSC with [Cu(**1**)(**5**)]$^+$ exhibits both a high capacitance and a relatively high recombination resistance, but also has the lowest R_t and the highest L_d/L of all the [Cu(**1**)(L$_{ancillary}$)]$^+$ dyes. This is reflected in the overall performance of this DSC.

The DSC with [Cu(**1**)(**6**)]$^+$ has the highest R_{rec}, but also the lowest capacitance which in combination with the highest R_t value (Table 9) will counteract the transport of the injected electrons, resulting in a relatively poor performance. In Table 8, it is interesting that the monosubstituted ligands **5** and **7** give rise to a higher capacitance, indicating that the asymmetric structure enhances electron injection into the TiO_2 leading to an increase in DSC efficiency. This is consistent with the photoconversion efficiences presented in Tables 2 and 6 and discussed earlier.

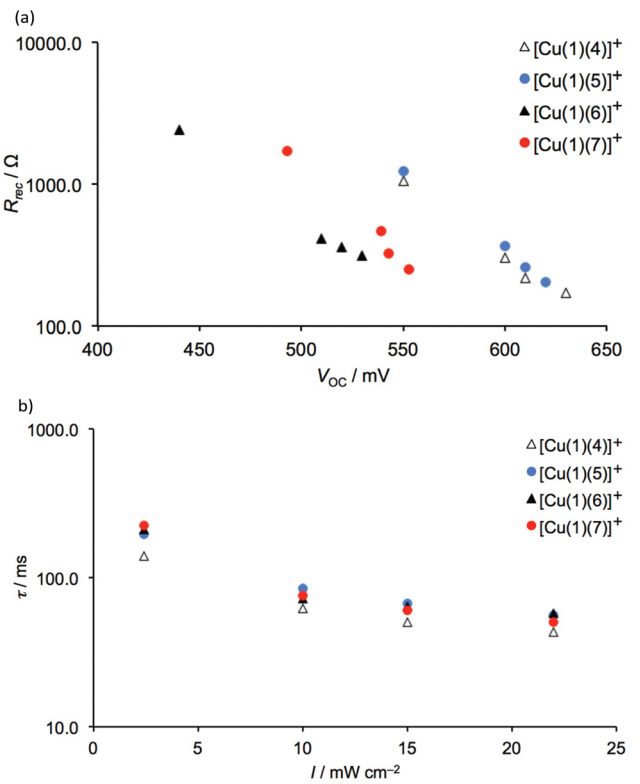

Fig. 14 (a) The recombination resistance as a function of V_{OC} and (b) the electron lifetime as a function of bias-light intensity in 3-day old DSCs containing dyes [Cu(**1**)(**4**)]$^+$, [Cu(**1**)(**5**)]$^+$, [Cu(**1**)(**6**)]$^+$, [Cu(**1**)(**7**)]$^+$.

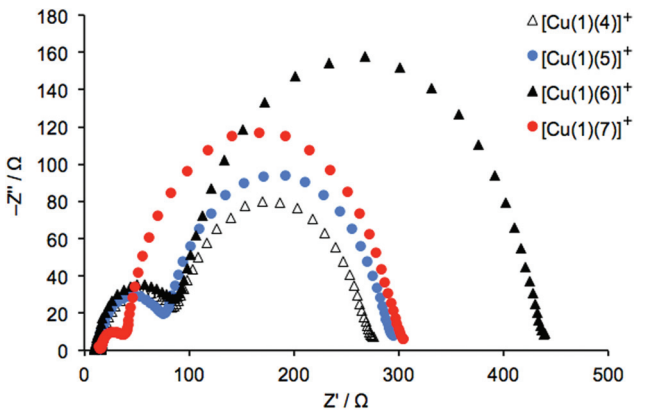

Fig. 15 Nyquist plots for 3-day old DSCs containing dyes [Cu(**1**)(**4**)]$^+$, [Cu(**1**)(**5**)]$^+$, [Cu(**1**)(**6**)]$^+$, [Cu(**1**)(**7**)]$^+$ measured with a bias-light intensity of 22 mW cm^{-2}.

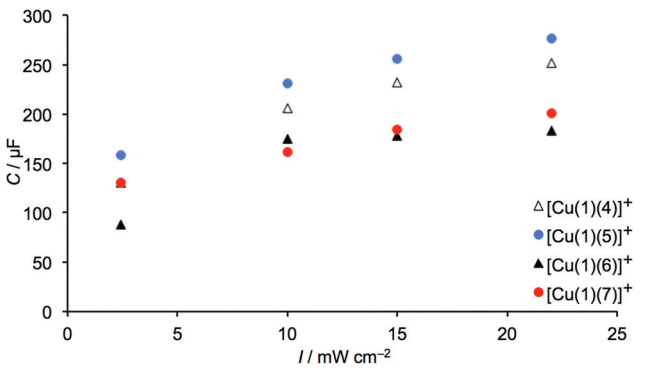

Fig. 16 Capacitance values of 3-day old DSCs containing dyes [Cu(**1**)(**4**)]$^+$, [Cu(**1**)(**5**)]$^+$, [Cu(**1**)(**6**)]$^+$, [Cu(**1**)(**7**)]$^+$.

EIS measurements: DSCs with different anchoring ligands

Fig. 17 shows values of R_{rec} and τ for DSCs with dyes containing anchors **2** and **3** (with thienyl-spacers) and ancillary ligands **5** and **7**. The value of V_{OC} (Tables 8 and 9) is highest in measurements for dyes with anchor **3**, consistent with conclusions based on *J–V* curves (see earlier discussion). Both the recombination resistance and the capacitance (Fig. 18) are higher for these dyes, and the transport resistance is lower. These factors all contribute to the higher photoconversion efficiencies of DSCs with dyes $[Cu(\mathbf{3})(\mathbf{5})]^+$ and $[Cu(\mathbf{3})(\mathbf{7})]^+$. As noted above, a higher R_t combined with a low R_{rec} limits the extent to which electrons are injected and at the same time, the resistance for the electron to recombine with the oxidized dye is low. This is the case for the measurements of DSCs with dyes containing anchor **2**, where L_d/L is lower than in its counterpart with **3**.

As discussed earlier and shown in eqn (4), a higher R_t may be accompanied by a higher E_{cb} which can reduce the charge injection efficiency. This will consequently decrease the V_{OC} due to a lower density of electrons in the conduction band. This is demonstrated in Table 9 by comparing data for $[Cu(\mathbf{2})(\mathbf{7})]^+$ and $[Cu(\mathbf{3})(\mathbf{7})]^+$; anchor **3** lowers R_t by ~60% and improves the V_{OC} by more than 20 mV. When the conduction band level is very high in a SC, resulting in a large R_t, the phenomenon is observed in an EIS measurement as Gerischer resistance in the mid-range frequency region. This is effectively displayed as a distorted semi-circle in the plot of $[Cu(\mathbf{2})(\mathbf{5})]^+$ in Fig. 19, where the EIS spectra from $[Cu(\mathbf{2})(\mathbf{5})]^+$ and $[Cu(\mathbf{3})(\mathbf{5})]^+$ are compared.

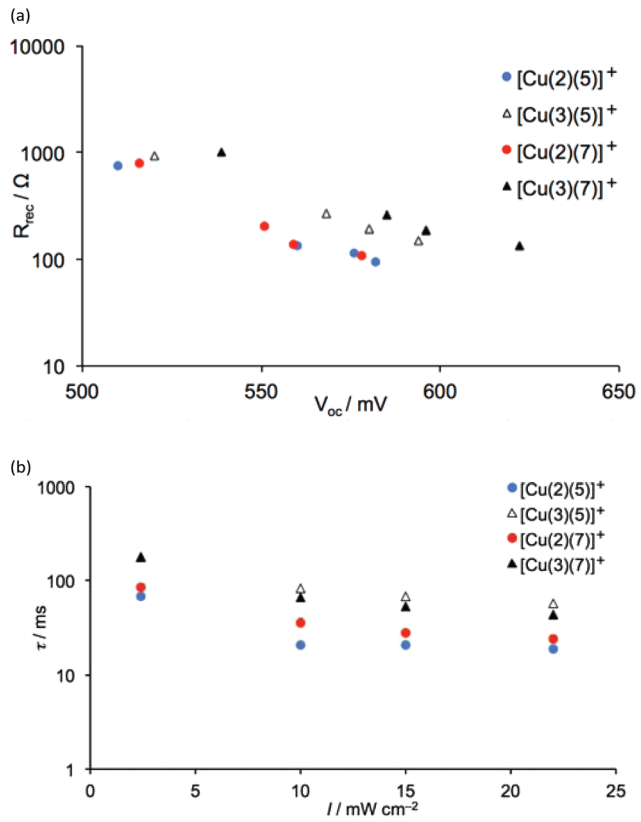

Fig. 17 (a) Plot of the recombination resistance against V_{OC}, and (b) the electron lifetime as a function of bias-light intensity of 3-day old DSCs containing dyes $[Cu(\mathbf{2})(\mathbf{5})]^+$, $[Cu(\mathbf{3})(\mathbf{5})]^+$, $[Cu(\mathbf{2})(\mathbf{7})]^+$ and $[Cu(\mathbf{3})(\mathbf{7})]^+$.

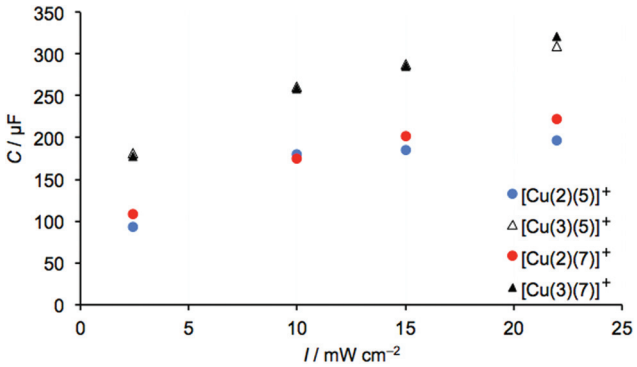

Fig. 18 Capacitance values of 3-day old DSCs containing dyes $[Cu(\mathbf{2})(\mathbf{5})]^+$, $[Cu(\mathbf{3})(\mathbf{5})]^+$, $[Cu(\mathbf{2})(\mathbf{7})]^+$ and $[Cu(\mathbf{3})(\mathbf{7})]^+$.

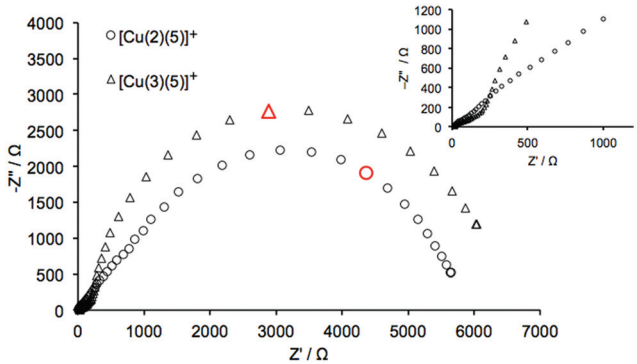

Fig. 19 Nyquist plots for $[Cu(\mathbf{2})(\mathbf{5})]^+$ and $[Cu(\mathbf{3})(\mathbf{5})]^+$ measured under a light intensity of 0.44 mW cm^{-2}. The data points shown in red were measured at 0.3 Hz. The inset shows an expansion of the data measured in the high-to-mid frequency region.

Conclusions

The current work extends our previous investigation of the favourable effects of introducing CF_3 groups into the ancillary ligands in $[Cu(L_{anchor})(L_{ancillary})]^+$ dyes in DSCs.[17] A change from CH_2Cl_2 to acetone in the dye-bath during on-surface assembly of the heteroleptic dyes $[Cu(\mathbf{1})(\mathbf{4})]^+$, $[Cu(\mathbf{1})(\mathbf{5})]^+$ and $[Cu(\mathbf{1})(\mathbf{6})]^+$ has only a small effect on DSC performance. The optimal dye in this series in terms of photoconversion efficiency and dye stability is $[Cu(\mathbf{1})(\mathbf{5})]^+$. Achieving enhancement of DSC performance by replacing the phenyl spacer in anchor **1** by a 2-thienyl unit is dependent upon the position of substitution of the phosphonic acid group in the thienyl ring. Improved V_{OC} is observed when the $PO(OH)_2$ anchor is in the 4- rather than 5-position (*i.e.* **3** is better than **2**). Similar values of V_{OC} are obtained on going from **1** to **3** with a given $L_{ancillary}$,

but on going from **1** or **3** to **2**, there is an ≈50–60 mV drop in V_{OC}; countering this, there is typically a gain in J_{SC} when **2** is used as L_{anchor}. The best photoconversion efficienies are obtained for the dye $[Cu(\mathbf{3})(\mathbf{5})]^+$ (η = 2.40% relative to a N719 reference of 5.76%).

The conclusions reached from plots of current-density (J) against potential (V), and external quantum efficiency spectra are supported by electrochemical impedance spectroscopic measurements. The EIS data showed that introducing CF_3 in place of Me substituents into $L_{ancillary}$ dramatically lowers the transport resistance, R_t, and increases C_μ; R_t decreases and C_μ increases when $L_{ancillary}$ is 6-substituted rather than 6,6′-disubstituted. In agreement with J–V curves, EIS data for DSCs with dyes containing **5** or **7** combined **2** or **3** reveal that use of **3** results in a significant enhancement in V_{OC} (particularly noteworthy when $L_{ancillary}$ = **7**). Furthermore, on going from $[Cu(\mathbf{3})(L_{ancillary})]^+$ to $[Cu(\mathbf{2})(L_{ancillary}]^+$, R_t is dramatically increased ($L_{ancillary}$ = **5** or **7**). Of the four dyes with thienyl spacers in the anchor that were tested, $[Cu(\mathbf{3})(\mathbf{5})]^+$ (which has the highest photoconversion efficiency) has the second highest capacitance as well as a rather high R_{rec} together and the next lowest R_t, indicating that electrons are readily injected into the conduction band; the recombination rate is such that a high V_{OC} results and, therefore, DSC performance improves.

Acknowledgements

We acknowledge the Swiss National Science Foundation (Grant number 200020_144500), the European Research Council (Advanced Grant 267816 LiLo), the Swiss Nano Institute (for the purchase of the EIS instrument), and the University of Basel for financial support. We thank Fabian Brunner and Sarah Keller for providing ligands, and Thomas Müntener for recording 600 MHz NMR spectra. Annika Büttner is thanked for providing the screen-printed electrodes, and we also acknowledge Dr Colin D. Martin for preliminary work on 4,4′-bis(thien-2-yl)-6,6′-dimethyl-2,2′-bipyridine. Res Jöhr and Drs Thilo Glatzel, Sebastian Fürer and Biljana Bozic-Weber are thanked for helpful discussions.

Notes and references

1 C. E. Housecroft and E. C. Constable, *Chem. Soc. Rev.*, 2015, **44**, 8386.
2 T. C. B. Harlang, Y. Liu, O. Gordivska, L. A. Fredin, C. S. Ponseca Jr., P. Huang, P. Chábera, K. S. Kjaer, H. Mateos, J. Uhlig, R. Lomoth, R. Wallenberg, S. Styring, P. Persson, V. Sundström and K. Wärnmark, *Nat. Chem.*, 2015, **7**, 883.
3 F. J. Malzner, S. Y. Brauchli, E. C. Constable, C. E. Housecroft and M. Neuburger, *RSC Adv.*, 2014, **4**, 48712.
4 M. Sandroni, L. Favereau, A. Planchat, H. Akdas-Kilig, N. Szuwarski, Y. Pellegrin, E. Blart, H. Le Bozec, M. Boujtita and F. Odobel, *J. Mater. Chem. A*, 2014, **2**, 9944.
5 M. Sandroni, M. Kayanuma, A. Planchat, N. Szuwarski, E. Blart, Y. Pellegrin, C. Daniel, M. Boujtita and F. Odobel, *Dalton Trans.*, 2013, **42**, 10818.
6 M. Sandroni, M. Kayanuma, M. Rebarz, H. Akdas-Kilig, Y. Pellegrin, E. Blart, H. Le Bozec, C. Daniel and F. Odobel, *Dalton Trans.*, 2013, **42**, 14628.
7 E. Schönhofer, B. Bozic-Weber, C. J. Martin, E. C. Constable, C. E. Housecroft and J. A. Zampese, *Dyes Pigm.*, 2015, **115**, 154.
8 B. Bozic-Weber, E. C. Constable, C. E. Housecroft, P. Kopecky, M. Neuburger and J. A. Zampese, *Dalton Trans.*, 2011, **40**, 12584.
9 P. Péchy, F. P. Rotzinger, Md. K. Nazeeruddin, O. Kohle, S. M. Zakeeruddin, R. Humphry-Baker and M. Grätzel, *J. Chem. Soc., Chem. Commun.*, 1995, 65.
10 K. Hanson, M. K. Brennaman, A. Ito, H. Luo, W. Song, K. A. Parker, R. Ghosh, M. R. Norris, C. R. K. Glasson, J. J. Concepcion, R. Lopez and T. J. Meyer, *J. Phys. Chem. C*, 2012, **116**, 14837.
11 B. Bozic-Weber, S. Y. Brauchli, E. C. Constable, S. O. Fürer, C. E. Housecroft, F. J. Malzner, I. A. Wright and J. A. Zampese, *Dalton Trans.*, 2013, **42**, 12293.
12 N. Armaroli, G. Accorsi, F. Cardinali and A. Listorti, *Top. Curr. Chem.*, 2007, **280**, 69.
13 C. E. McCusker and F. N. Castellano, *Inorg. Chem.*, 2013, **52**, 8114.
14 S. Y. Brauchli, F. J. Malzner, E. C. Constable and C. E. Housecroft, *RSC Adv.*, 2015, **5**, 48516.
15 A. Büttner, S. Y. Brauchli, R. Vogt, E. C. Constable and C. E. Housecroft, *RSC Adv.*, 2016, **6**, 5205–5213.
16 See for example: A. Abbotto and N. Manfredi, *Dalton Trans.*, 2011, **40**, 12421; L. Zhang and J. M. Cole, *ACS Appl. Mater. Interfaces*, 2015, **7**, 3427; P. Kumaresan, S. Vegiraju, Y. Ezhumalai, S. L. Yau, C. Kim, W.-H. Lee and M.-C. Chen, *Polymers*, 2014, **6**, 2645; A. Mishra, N. Pootrakulchote, M. K. R. Fischer, C. Klein, Md. K. Nazeeruddin, S. M. Zakeeruddin, P. Bäuerle and M. Grätzel, *Chem. Commun.*, 2009, 7146.
17 F. Brunner, M. Klein, S. Keller, C. D. Morris, A. Prescimone, E. C. Constable and C. E. Housecroft, *RSC Adv.*, 2015, **5**, 58694.
18 B. Bozic-Weber, V. Chaurin, E. C. Constable, C. E. Housecroft, M. Meuwly, M. Neuburger, J. A. Rudd, E. Schönhofer and L. Siegfried, *Dalton Trans.*, 2012, **41**, 14157.
19 *APEX2, version 2 User Manual, M86-E01078*, Bruker Analytical X-ray Systems, Inc., Madison, WI, 2006.
20 P. W. Betteridge, J. R. Carruthers, R. I. Cooper, K. Prout and D. J. Watkin, *J. Appl. Crystallogr.*, 2003, **36**, 1487.
21 I. J. Bruno, J. C. Cole, P. R. Edgington, M. K. Kessler, C. F. Macrae, P. McCabe, J. Pearson and R. Taylor, *Acta Crystallogr., Sect. B: Struct. Sci.*, 2002, **58**, 389.
22 C. F. Macrae, I. J. Bruno, J. A. Chisholm, P. R. Edgington, P. McCabe, E. Pidcock, L. Rodriguez-Monge, R. Taylor, J. van de Streek and P. A. Wood, *J. Appl. Crystallogr.*, 2008, **41**, 466.
23 F. Kröhnke, *Synthesis*, 1976, 1.

24 V. Spampinato, N. Tuccitto, S. Quici, V. Calabrese, G. Marletta, A. Torrisi and A. Licciardello, *Langmuir*, 2010, **26**, 8400 and references therein.
25 G. R. Desiraju and T. Steiner, *The Weak Hydrogen Bond in Structural Chemistry and Biology*, Oxford University Press, 1999, p. 5.
26 H. J. Snaith, *Energy Environ. Sci.*, 2012, **5**, 6513.
27 H. J. Snaith, *Nat. Photonics*, 2012, **6**, 337.
28 F. J. Malzner, S. Y. Brauchli, E. Schönhofer, E. C. Constable and C. E. Housecroft, *Polyhedron*, 2014, **82**, 116.
29 S. Y. Brauchli, F. J. Malzner, E. C. Constable and C. E. Housecroft, *RSC Adv.*, 2014, **4**, 62728.
30 X. Chen, C. Jia, Z. Wan, J. Feng and X. Yao, *Org. Electron.*, 2014, **15**, 2240.
31 Q. Wang, J. E. Moser and M. Grätzel, *J. Phys. Chem. B*, 2005, **109**, 14945.
32 I. S. Yahia, H. S. Hafez, F. Yakuphanoglu, B. F. Senkal and M. S. A. Abdel Mottaleb, *Synth. Met.*, 2011, **161**, 1299.
33 R. Kern, R. Sastrawan, J. Ferber, R. Stangl and J. Luther, *Electrochim. Acta*, 2002, **47**, 4213.
34 J.-L. Lan, T.-C. Wei, S.-P. Feng, C.-C. Wan and G. Cao, *J. Phys. Chem. C*, 2012, **116**, 25727.
35 J. Bisquert and F. Fabregat-Santiago, in *Dye-Sensitized Solar Cells*, ed. K. Kalyanasundaram, EPFL Press, 2010, p. 492.
36 J. Bisquert, F. Fabregat-Santiago, I. Mora-Seró, G. Garcia-Belmonte and S. Gimènez, *J. Phys. Chem. C*, 2009, **113**, 17278.
37 F. Fabregat-Santiago, J. Bisquert, G. Garcia-Belmonte, G. Boschloo and A. Hagfeldt, *Sol. Energy Mater. Sol. Cells*, 2005, **87**, 117.